

# Average Rated Torque Calculations for Switched Reluctance Machines Based on Vector Analysis

*Aleksas Stuikys and Jan Sykulski*

## Abstract

An average rated torque estimation for generally saturable switched reluctance (SR) machines based on vector analysis is described. The proposed analytical method enables the switched reluctance machine designers to compute quickly and relatively accurately the rated torque of the machine. This approach offers simplicity, accuracy, and intuitive insight characteristic to analytical solutions of magnetically nonlinear problems otherwise achievable only with time-consuming computer-based numerical simulation tools. The suggested analytical methodology, therefore, offers immediate answers regarding the rated torque performance at the early stages of the machine sizing and design process. In this chapter, the switched reluctance machine rated torque calculation is derived based on the analytically estimated flux-linkage characteristic map and the knowledge of the DC bus voltage of the machine. It is further demonstrated that the proposed analytical rated torque calculations, based on vector analysis, enable construction of highly accurate instantaneous phase current profiles using a graphical method and thus aiding intuition and providing valuable insight into the nonlinear switched reluctance machine operation and control requirements. The proposed method will be found particularly suitable for those studying the nonlinear design and control of switched reluctance machine technologies for electric vehicle traction and industrial applications.

**Keywords:** analytic average torque calculation, vector analysis, nonlinear switched reluctance machines

## 1. Introduction

Since the dawn of the popularity of the switched reluctance (SR) motors [1], many diverse developments of this machine's technology have resulted, including theoretical analysis, and the volume of the published literature on these topics is enormous. For this reason it would be impossible to encompass the entire range of published methods of analysis and design of SR motors, let alone to effectively utilize them in the machine design process. Therefore the aim of this work is to provide the readers with the essential analytical formulae and methodologies in order to allow them to analyze quickly and relatively accurately a desired SR machine for a particular application.

Since the principle of operation of SR machines does not require any permanent magnets for the production of torque, such machines offer an excellent alternative electric motor technology at this moment in time in the context of the cost and environmental impact uncertainties of permanent magnet materials [2]. Usually, the SR motor will be designed to operate from a fixed DC voltage supply, such as a battery, and the stator windings of the machine will be of the concentrated type. A typical structure of an SR electric motor or generator is shown in **Figure 1**.

In **Figure 1** the depicted machine contains 18 stator poles and 12 rotor poles; therefore this particular SR machine configuration is abbreviated as an 18/12 SR motor. Therefore, with the knowledge of these variables, we are able to compute the number of “steps” the rotor will make in a single revolution as it gets aligned to each of the energized stator poles, as in Eq. (1):

$$\text{number of rotor steps} = m \cdot N_r \quad (1)$$

where  $m$  is the number of phases and  $N_r$  is the number of rotor poles. For the 18/12 configuration, Eq. (1) gives 36 steps. Therefore, the rotor will make 36 steps from one stator pole to the next in one complete revolution.

For the SR machine to operate effectively, it requires a capable high power and switching frequency power electronic converter in order to shape the phase current waveforms to be fed into the SR machine phase windings. The most general power electronic converter structure used for SR machines, known as the asymmetric half-bridge converter, is shown diagrammatically in **Figure 2**.

The power electronic converter for the three-phase 18/12 SR machine is assumed to be connected to a fixed magnitude DC bus voltage  $V$ . Each phase of the machine is connected to two power transistor switches,  $T1$  and  $T2$ , and two power diodes,  $D1$  and  $D2$ , in an asymmetric h-bridge configuration. The transistor switches are active devices, and therefore in order to control their conduction states and switching speed, the electronic signals are used:  $sig1$  and  $sig2$ . The power diodes are passive components, and therefore they do not require electronic signals in order to work. The capacitor  $C$  is connected across the DC bus supply voltage lines to be used as an energy dump capacitor.

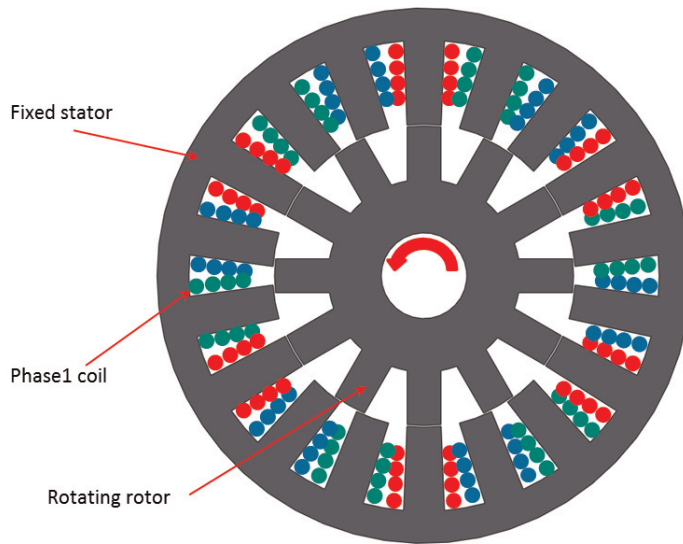


**Figure 1.**  
Cross-sectional view of the electromechanical structure of a three-phase 18/12 switched reluctance machine.

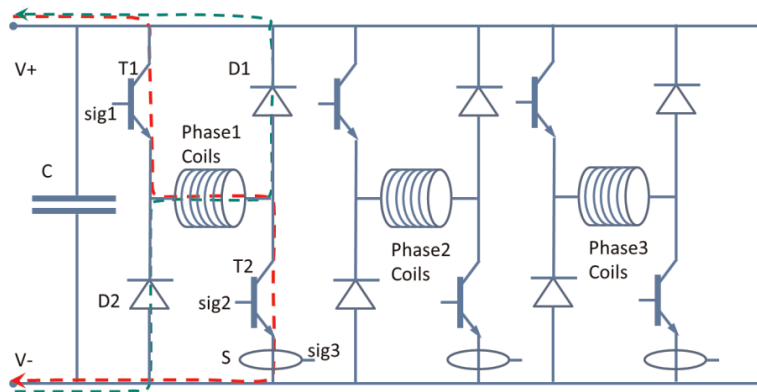


**Figure 2.**  
 H-bridge asymmetric power electronic converter for the three-phase 18/12 SR machine.

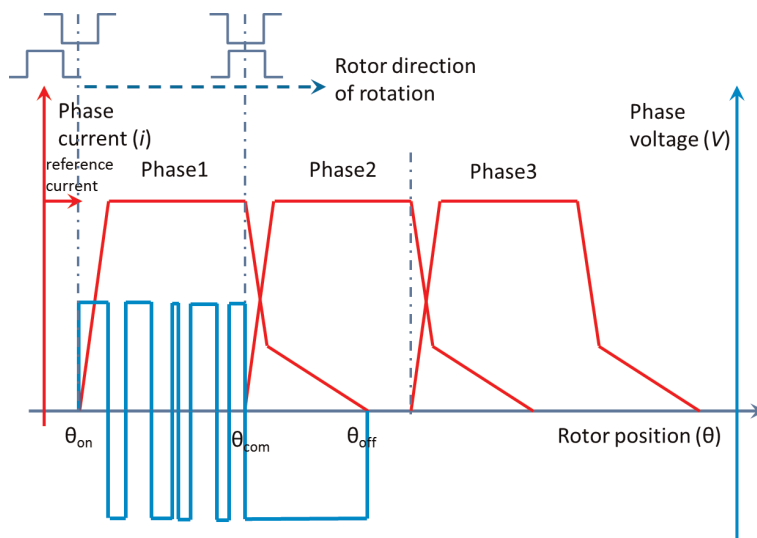


**Figure 3.**  
 Phase current profiles in the phase windings resulting from the voltage switching strategy of the asymmetric h-bridge converter.

The sequence of operation of the h-bridge converter in terms of phase current profiles as shown in **Figure 3**—for the motoring mode of the SR machine—is as follows. Assuming the hard chopping voltage switching strategy to begin with, when the rotor pole is furthest away from the stator pole, the two power transistor switches are latched so as to enable the conduction of the current. This action results in the electric current flow from the positive supply terminal, through the phase windings, to the negative terminal, as represented by the red dashed line in **Figure 2**, with the arrow indicating the direction of the flow. Once the current has reached some predetermined reference value, say peak rated current, the signal from the current sensor *S* is sent to the electronic controller (not shown) of the SR machine which, in turn, sends signals to the power transistors, *T1* and *T2*, in order to switch them off, so as to stop the flow of the current. This last action, however, does not stop the circulation of current in the phase winding immediately since the magnetic field, created by the currents, prevents the current from reducing to zero instantly. Moreover, exactly at the same time, the power diodes start to conduct current in the phase winding, as shown by the green dashed line in **Figure 2**, with the arrow indicating the direction of the current flow. From this operation we deduce that the current in the

phase winding does not alternate and is therefore a direct current (DC). The resulting current profile is shown schematically in **Figure 3**.

From **Figure 3** it may be seen that once the current reaches some specified value, the electronic controller has to check the value of the measured current by the current sensor  $S$  in the winding, so as to keep it constant up until the commutation angle  $\theta_{com}$ , at which point both transistors are switched off. The current profile from  $\theta_{com}$  to  $\theta_{off}$  is a result of the power diodes' action, represented by the green dashed line in **Figure 2**. At this stage it becomes clear why the dump capacitor  $C$  is used in h-bridge converters: because the magnetic energy established by the current circulating in the winding is not fully used up, it has to be returned in the form of a current back into the supply; however, in order to keep the supply undisturbed, the capacitor  $C$  in **Figure 2** is used to absorb the returning energy. The entire switching process is repeated for the other phases of the SR machine as shown in **Figures 2** and **3**, where generally the overlap of each of the three phase current profiles will depend on the timing of the transistor switching action as well as on the operating speed of the machine and the torque requirement at that speed.

It should be noted here that the analytical rated torque calculations presented below are based on the assumption that the correct switching mode of the power electronic converter is assumed first. Furthermore, the actual performance of an SR machine can be greatly affected by the design choice of the power converter topology and the switching action, including the torque production and the energy conversion efficiency of the device [3]. Therefore, the following analytical solutions will be based on the "hard chopping" voltage switching strategy as in **Figure 3** for the asymmetric half-bridge converter presented in **Figure 2**.

The particular SR motor considered in this chapter is taken from [4]. The main reason behind the decision to use a published SR machine design was that it had been extensively optimized, its performance was analyzed, and it was actually built and tested in order to verify the results. Finally, the published work should be of reproducible quality, and therefore the chosen SR machine design makes an excellent choice when comparing the validity of the proposed analytical solution with the solutions obtained from extensive computer simulations and carefully controlled experimental measurements.

The chosen 50 kW SR motor parameters to be used in the present analysis are given in **Table 1**.

By application of the open license finite element method [5] to the magnetic analysis of the chosen SRM2 design, the aligned and the unaligned rotor positions are analyzed in terms of the magnetic flux distributions in the magnetic circuit of the device, as shown in **Figures 4** and **5**.

**Figures 4** and **5** are used to describe the fundamental theory of SR machines in terms of the phase flux-linkage.

Therefore, if we consider the amount of magnetic flux  $\Phi$ , measured in units of weber, being established in the stator pole around which the number of conductors  $N$  is wound in the concentrated manner as in **Figure 1**, then the flux-linkage thus created is given in Eq. (2):

$$\Psi = N \cdot \Phi(V \cdot s) \quad (2)$$

where instead of the intuitive units of weber-turns, we choose to use the volt-seconds (as a derived SI unit) since this unit of measurement will be very handy when we explain the significance of the flux-linkage in the SR machine analysis section. Furthermore, the phase flux-linkage computed in Eq. (2) is multiplied by the number of the coils connected in series,  $N_s$ , to obtain the total flux-linkage for that particular phase.

SR motor design variables and test results	
Design parameters	50 kW SRM2
Outer diameter [mm]	269
Stack length [mm]	135
Air gap length [mm]	0.5
Iron core material	10JNEX900
Wire diameter [mm]	0.6
Wire turns [turns]	17
Wire parallel turns [turns]	22
Slot fill factor [%]	57.0
Stator pole arc angle $\beta_s$ [degrees]	10.5
Rotor pole arc angle $\beta_r$ [degrees]	11
Rated angular speed [rpm]	1200
Current, peak [A]	320
Max. current density [A/mm <sup>2</sup> ]	33 (33)
RMS current (@1200 rpm) [Arms]	204 (206)
Max. torque (@1200 rpm) [Nm]	415 (400.4)
Number of phases	3
DC bus voltage [V]	500
Max. power [kW]	50

( ) denotes test results.

**Table 1.**  
50 kW SR machine parameters, adapted from [4].

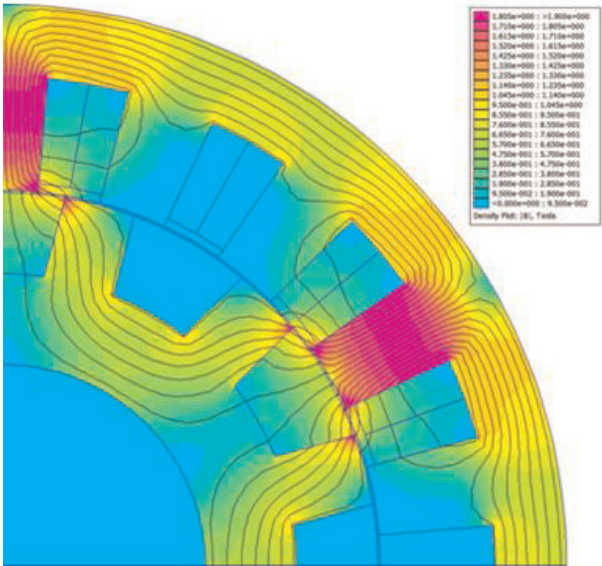


**Figure 4.**  
Magnetic flux distribution and flux density in the switched reluctance machine for the unaligned rotor position.



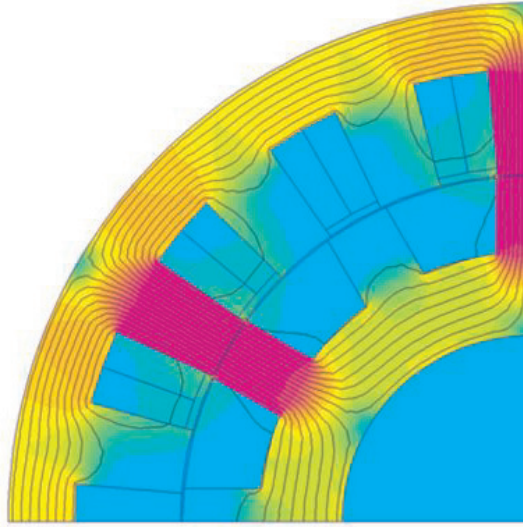


**Figure 5.**  
Magnetic flux distribution and flux density in the switched reluctance machine for the aligned rotor position.

Using the same reasoning as above; Eq. (2) will apply for the unaligned rotor position as well as for the aligned case as shown in **Figures 4 and 5**. In fact Eq. (2) is used to compute the flux-linkage for any rotor angular position with respect to the stationary stator. One further outcome we are able to accomplish—in addition to varying the rotor angular position to compute the flux-linkage for that rotor position—is to vary the phase current that is being circulated in the concentrated winding of the stator pole. Therefore, if we increase the current from zero to its full rated peak value (see **Table 1**), for each of the rotor positions from the fully aligned to the fully unaligned, in steps of 1 mechanical degree, the complete flux-linkage map of the 18/12 SR machine will result, as plotted in **Figure 6**.

Some highly notable observations of **Figure 6a** are that for the aligned rotor position, the flux-linkage builds up very quickly for the range of currents, after which it levels off considerably; this occurs in the region of 80 (amps) called the magnetic saturation point. The unaligned rotor position flux-linkage is fairly linear for the entire range of the phase current values, especially if compared to the fully

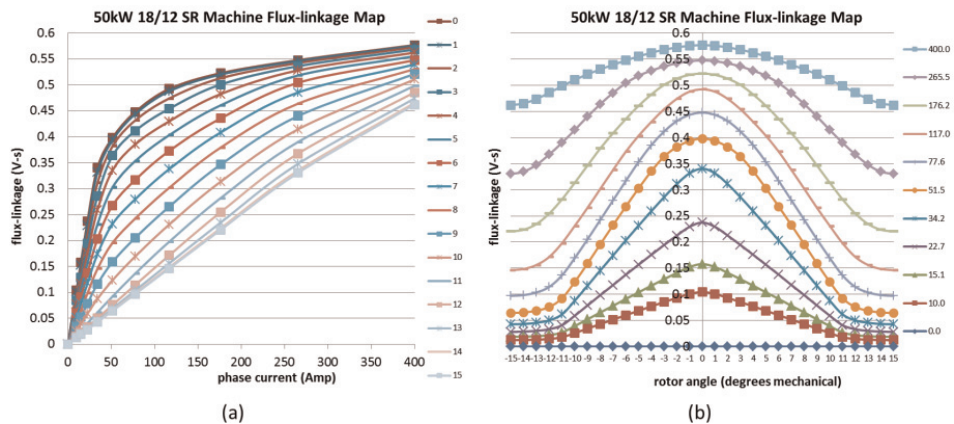


**Figure 6.**  
Flux-linkage map for the 18/12 SR machine; (a) taking the rotor position as a parameter, (b) taking the phase current as a parameter.

aligned position. The intermediate rotor position flux-linkage curves, generally speaking, become highly nonlinear as the rotor tends toward the fully aligned position. If the flux-linkage curves with respect to the rotor position are examined taking the phase current as a parameter, as in **Figure 6b**, it may be seen that linearity is not present at all, and for a given current value, the flux-linkage value will vary with respect to all rotor positions from the fully unaligned to the fully aligned. This is true irrespective of the rotor rotation in clockwise or counterclockwise direction, as in **Figure 6b**.

The torque production of the SR machine can be described in terms of the flux-linkage map shown in **Figure 6a**. If we were to consider only the fully aligned and unaligned rotor position flux-linkage curves, as in **Figure 7**, then it would follow that as the rotor tends toward the fully aligned position, the current build-up in the phase winding would increase the stored magnetic field energy  $W_f$ . The phase current would then follow the same profile as in **Figure 3**, yet this time it is shown with respect to the flux-linkage curves in **Figure 7** (red dashed).

As can be seen from the graphical representation, the magnetic co-energy  $W'$  is represented by the area bound by the aligned and the unaligned flux-linkage curves and therefore is given by Eq. (3) in terms of the aligned flux-linkage:

$$W' = \int_0^i \Psi di \text{ (Joules)} \quad (3)$$

Thus, generally, if the magnetic field co-energy is created as a result of the rotor moving from the unaligned to the aligned position, while the phase current is kept constant, the torque generated,  $T$ , can be computed as in Eq. (4):

$$T = \left[ \frac{\partial W'}{\partial \theta} \right]_{i=\text{constant}} \text{ (N} \cdot \text{m)} \quad (4)$$

Therefore, for a given SR machine, we are interested in maximizing the area  $W'$  in order to arrive at a torque dense machine design. This is possible to achieve effectively if the aligned rotor position flux-linkage curve is maximized for all phase current values, while the unaligned rotor position flux-linkage curve is minimized for a given SR machine. Furthermore, the phase current profile itself will determine the magnitude of  $W'$  created, providing the phase current locus encompasses as much of the area as possible, as shown in **Figure 7**.

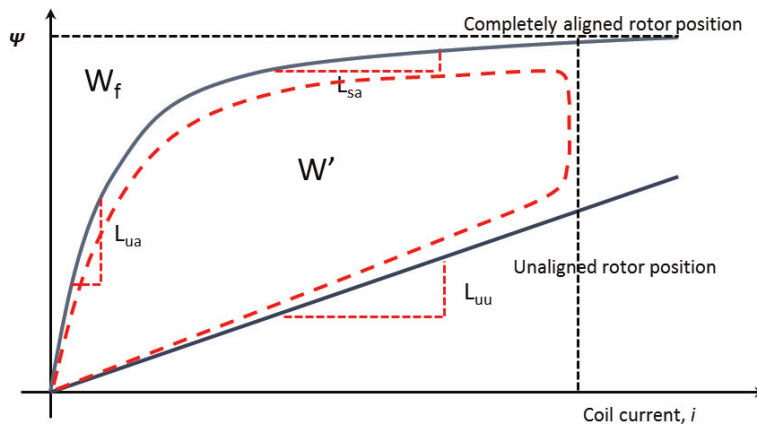


**Figure 7.**  
 Magnetic field energy  $W_f$  and co-energy  $W'$  representation.

The published and generally accepted phase torque calculations were based on the assumption of a linear machine theory, thus assuming non-saturating SR machine flux-linkage curves and their associated unsaturated aligned  $L_{ua}$  and unsaturated unaligned  $L_{uu}$  inductances, as shown in **Figure 8a**. The alternative to the linear theory is the nonlinear flux-linkage curves theory [6], with the additional saturated aligned inductance  $L_{sa}$ , in which  $W'$  is represented by the parallelogram area the phase current locus encompasses, as shown in **Figure 8b**.

From **Figure 8a** it is seen that the co-energy area  $W'$  is represented by the triangle and therefore is given as in Eq. (5):

$$W' = \frac{1}{2} \Psi \cdot i = \frac{1}{2} (L_{ua} - L_{uu}) i^2 \text{ (Joules)} \quad (5)$$

where  $L$  is an inductance which defines the slope of the particular linearized flux-linkage curve from **Figure 6a** as in **Figure 8a** at a particular rotor position and the peak value  $i$  of the flat-topped current profile. The torque produced by such a non-saturating SR machine will be given as in Eq. (6):

$$T = \frac{1}{2} i^2 \frac{dL}{d\theta} (N \cdot m) \quad (6)$$

which is the same as Eq. (5) being divided by the rotor angle that is being turned.

The torque production for the saturating flux-linkage curves producing parallelogram area of magnitude  $W'$  in **Figure 8b** is given in Eq. (7) [6]:

$$W' = V \frac{c \cdot \beta s}{\omega} \cdot i \left[ 1 - \frac{1}{2s} \right] \text{ (Joules)} \quad (7)$$

where  $c$  is commutation factor,  $s$  is combined inductance ratio,  $\beta s$  is stator pole arc angle as in **Table 1**,  $V$  is the DC bus voltage,  $\omega$  is rotor angular speed, and Eq. (7) is applicable only when  $L_{sa} = L_{uu}$ .

In general, the non-saturating SR machine is rather a special case of the generally saturating SR machine and for this reason will not deliver as high a torque value as is otherwise potentially possible with the saturating SR machine, since the area  $W'$  will be much lower for the given rated current at a specified speed of the machine. The saturating SR machine with the assumed co-energy area  $W'$  represented by the

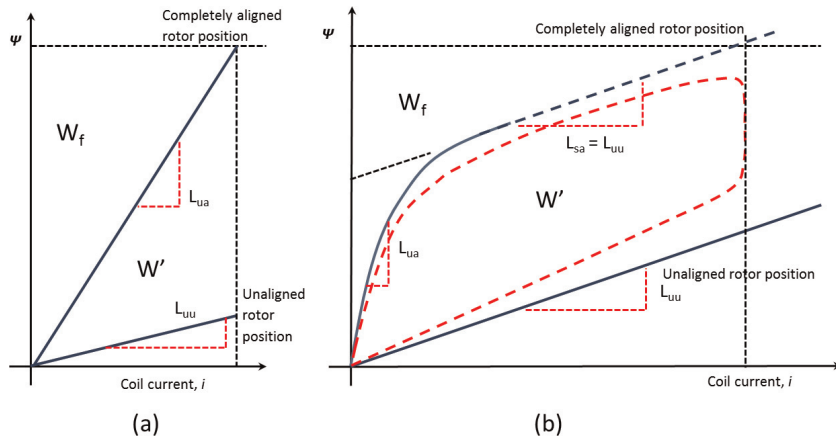


**Figure 8.** Linear flux-linkage and torque production theory (a), nonlinear flux-linkage and torque production theory based on parallelogram area (b).



parallelogram area, as in **Figure 8b**, is not very accurate since in practical SR machine devices  $L_{sa} \neq L_{uu}$ , which is the slope in **Figure 8b**, since the performance envelope of SR machines, in terms of the inductance ratios, is limited to the following bounds [7]:

$$6 < \frac{L_{ua}}{L_{uu}} < 14 \quad (8)$$

These bounds indicate that a fully saturable SR machine having the inductance ratio of less than 6 is considered to be unsuitable as it will not be a torque dense machine. On the other hand, the inductance ratio of 10 or more in Eq. (8) will indicate exceptionally high torque density SR machine capable of high instantaneous torque production, which is most desirable. It follows that our SRM2 design, from **Figure 6**, is capable of a reasonable torque production since the inductance ratio is about 8. However, achieving the inductance ratio of more than 10 is not a simple task, calling for highly specialized computer-based multi-objective optimization routines that are computationally intensive [8], and is therefore beyond the scope of the treatment in this chapter.

Going back to the previously stated argument regarding the assumed  $W'$  based on the parallelogram area calculation with Eq. (7), from **Figure 8b** it is evident that the saturated aligned flux-linkage curve has the same slope  $L_{sa}$  as the unsaturated unaligned flux-linkage curve slope  $L_{uu}$ . Comparing these two parallel inductance flux-linkage curves in **Figure 8b** with the corresponding curves of our SRM2 design of **Figure 6a** reveals that the parallel inductance assumption is inaccurate. Therefore, in general, the parallelogram theory-based torque computations, as in Eq. (7), for the saturable SR machine can lead to underestimated values, unless some scaling factor is introduced to compensate for the discrepancy resulting from the parallelogram area assumption applied to the nonparallel inductances. It will be shown that the two methods of Eqs. (5) and (7) are both special cases of the general torque production model based on quadrilateral area computation that is proposed in this chapter.

## 2. General analytic theory for saturable switched reluctance machines

In this chapter we set out the proposed nonlinear theory based on vector analysis of quadrilaterals for the SR machines. By presenting the nonlinear theory, it will be demonstrated how to estimate the average rated torque at the rated angular speed of the SR machine taking into account the magnetic nonlinearity of the magnetic circuit of the machine. The nonlinear theory will also be used to construct the instantaneous current profiles at the rated angular speed of the machine as well as to estimate the average phase current and voltage. The proposed nonlinear theory is also applicable to the generator mode of the SR machine, and the presented examples will demonstrate the results. Finally, the nonlinear analytical theory enables the estimation of the power electronic converter volt-ampere requirements of the switched reluctance machine as well as the energy conversion ratio for the machine. All these estimates will be used to construct the estimated speed-torque envelopes for the analyzed saturable SR machine, thus concluding the preliminary design process of the device using the analytical theory.

### 2.1 Switched reluctance machine energy conversion estimation and flux-linkage map construction

Since the flux-linkage map of an SR machine is the main piece of information to be used for the torque production estimation, the already constructed complete

flux-linkage map for the selected SRM2 machine design is redrawn again, this time for the aligned and the unaligned curves only, as shown in **Figure 9**.

In **Figure 9** the flux-linkage curves are first drawn from the finite element analysis-obtained data points of **Figure 6a**, assuming that  $L_{sa} \neq L_{uu}$ . The three linear curves are obtained by splitting the aligned flux-linkage curve in the region of the saturation point, at approximately 80 A current point in this case; however, the two parts of the split aligned flux-linkage curve are overlapping in order to facilitate more accurate linear fit. The linear fit of the unaligned flux-linkage curve also indicates that the linear fit is a very close approximation, as can be inferred from the statistical goodness of fit measure  $R^2$ , the value of which in **Figure 9** for the linear flux-linkage is very close to unity. It is noted at this point that all of the linearized fits are rather subjective; however, the aim to keep the area  $W'$  in **Figure 7** as close to the area bound by the linearized curve fits in **Figure 9** will ensure that our subsequent calculations will be accurate.

Having obtained the satisfactory linearization of the curves, as in **Figure 9**, we now define the following flux-linkage expressions (units of which can be in *volt-seconds* or *weber*) in terms of the known inductances and phase current  $i$ .

Unsaturated unaligned flux-linkage:

$$\Psi_{uu} = L_{uu} \cdot i = 0.0012072 \cdot i \quad (9)$$

Unsaturated aligned flux-linkage:

$$\Psi_{ua} = L_{ua} \cdot i_s = L_{sa} \cdot i_s + \Psi_s = 0.0071879 \cdot i_s = 0.0004948i_s + 0.4192920 \quad (10)$$

Saturated aligned flux-linkage:

$$\Psi_{sa} = L_{sa} \cdot i_r + \Psi_s = 0.0004948i_r + 0.4192920 \quad (11)$$

where  $i_r$  is the rated phase current, as given in **Table 1**, and is equal to 320 A for the selected SRM2 design.

The saturation current,  $i_s$ , is found from Eq. (10) since the two lines intersect:

$$i_s = \frac{\Psi_s}{L_{ua} - L_{sa}} = \frac{0.4192920}{0.0071879 - 0.0004948} \approx 62.6 \text{ (A)} \quad (12)$$

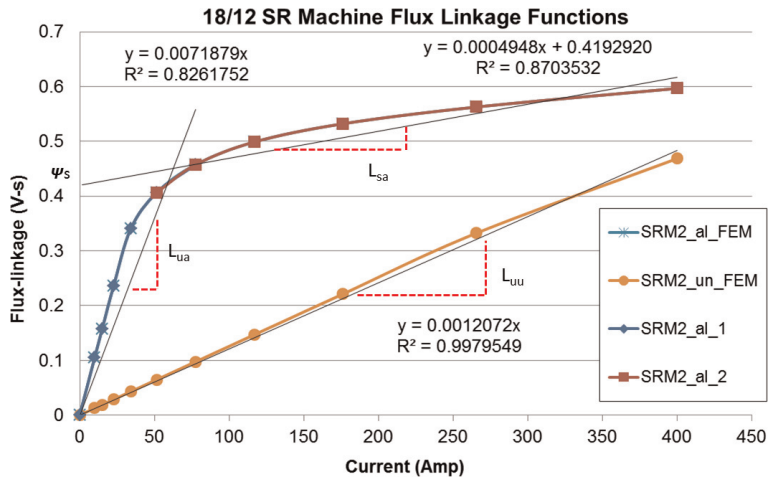


**Figure 9.** Flux-linkage curves for the 18/12 SRM2, taking the rotor position as the parameter and the linearized fits.



Eq. (15) is only convenient if the flux-linkage and the current quantities are known numerically at the required points on the quadrilateral. Usually it is preferred to work with the inductances  $L$  and the rated current value, since these quantities are used for other electric machines and therefore can be more intuitive in the SR machine design process as well.

Substituting the inductance relations, Eq. (9) to (13), into Eq. (15) and simplifying yield

$$\begin{aligned} W' &= \frac{1}{2} [(L_{ua} \cdot i_s) i_r - (L_{uu} \cdot i_r) i_r - (L_{sa} \cdot i_r + \Psi_s) i_s + (L_{sa} \cdot i_r + \Psi_s) i_r] \\ &= \frac{1}{2} [(L_{sa} - L_{uu}) i_r^2 + (L_{ua} - L_{sa}) i_s i_r + \Psi_s i_r - \Psi_s i_s] \end{aligned} \quad (16)$$

Eq. (16) is not yet the preferred final formula for the area calculation since we wish to eliminate the numerical flux-linkage values  $\Psi_s$ , and the saturation current  $i_s$ , and leave only the rated phase current values and inductances. Also we note at this stage of derivation that if the rated current were to reduce to such a point so as to coincide with the saturation current in Eq. (16), the resulting area  $W'$  would be equal to the area found in Eq. (5) for the non-saturating SR machine, since all but the first term in the brackets would cancel out. Therefore the area calculation with Eq. (16) is the general case, whereas Eq. (5) is the special case as was noted earlier.

Considering **Figure 9** and Eq. (16), we draw yet two more corresponding diagrams: one for the flux-linkage quadrilateral as in **Figure 11** and another for the phase current profile as in **Figure 12**.

**Figure 11** shows that, generally, the SR machine phase current commutation starts well before the fully aligned position [6], at point C instead of point B, since it would require an infinite DC bus voltage in order to bring the phase current to zero instantly so as to avoid the negative torque production which is undesirable in the motoring mode. Therefore the current will decay to point E before reaching zero value as before in **Figure 10**. The line AC in **Figure 11** can be expressed in terms of the inductances in Eqs. (9) and (11) and introducing the commutation factor  $c$ , being in the region of  $0 < c \leq 1$ , which is also shown in **Figure 11**:

$$AC = c \cdot AB = L_{sa} \cdot i_r + c \Psi_s - L_{uu} \cdot i_r; (V \cdot s) \quad (17)$$

since the unaligned unsaturated inductance is not affected by the commutation factor  $c$ , as in **Figure 11**.

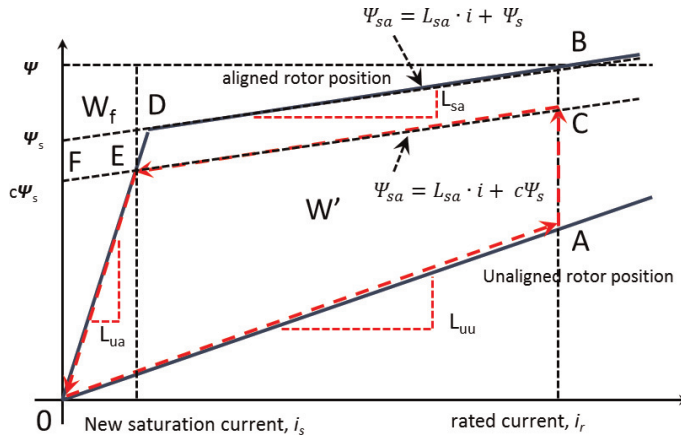


**Figure 11.** Linearized flux-linkage curves for the 18/12 SRM2 and the reduced phase current locus (dashed red).

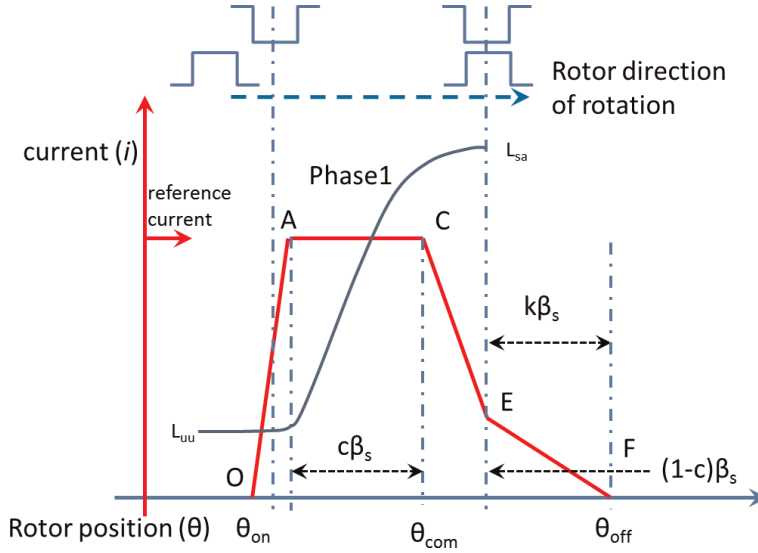


**Figure 12.**  
 Phase current profile in the phase windings resulting from the assumed linearized current profile in **Figure 11**.

The units of volt-seconds of the flux-linkage difference  $AC$  in **Figure 11** now comes very handy since if we know the angular speed of the SRM2 machine  $\omega$  (radians/second) and the stator pole arc angle,  $\beta_s$  (radians), both as specified in **Table 1**, then Eq. (17) can be expressed in terms of the root-mean-square voltage  $V_{rms(PWM)}$  applied to the phase winding from  $A$  to  $C$ , in order to maintain the phase current flat-topped, as in **Figure 11**:

$$AC = c \cdot AB = L_{sa} \cdot i_r + c\Psi_s - L_{uu} \cdot i_r = V_{rms(PWM)} \frac{c \cdot \beta_s}{\omega}; (V \cdot s) \quad (18)$$

the last term in Eq. (18) indicating that the units of  $(V \cdot s)$  result if the rotor rotates by the angle  $c \cdot \beta_s$  when rotating at the angular speed  $\omega$ , while simultaneously the voltage  $V_{rms(PWM)}$  is applied across the phase winding. The  $V_{rms(PWM)}$  is the voltage needed to counteract the build-up of the back-electromotive force, *back-emf*, being generated in the phase windings at the specific speed.

Rearranging Eq. (18) in order to obtain the saturation flux-linkage constant in **Figure 11** gives

$$\Psi_s = V_{rms(PWM)} \frac{\beta_s}{\omega} - (L_{sa} - L_{uu}) \cdot \frac{i_r}{c} \quad (19)$$

Since the equality previously considered in Eq. (10) has changed as a result of the early commutation, it is rewritten here for convenience:

$$L_{ua} \cdot i_s = L_{sa} \cdot i_s + c \cdot \Psi_s \quad (20)$$

since the two linearized curves intersect at point  $E$  in **Figure 11**.

To obtain the new saturated phase current value  $i_s$ , remembering to include the phase commutation factor  $c$ , Eq. (20) is rearranged:

$$i_s = \frac{c \cdot \Psi_s}{L_{ua} - L_{sa}}, \quad (21)$$

and by using the result from Eq. (19), the saturation current, Eq. (21), can be expressed as

$$i_s = \frac{V_{rms(PWM)} \frac{c \cdot \beta s}{\omega} - (L_{sa} - L_{uu}) i_r}{L_{ua} - L_{sa}} \quad (22)$$

Therefore, having obtained Eq. (19) and (22), we are now in the position to express the co-energy  $W'$  given in Eq. (16) in terms of the inductances, the voltage, the rated phase current, the angular speed, and the stator pole arc angle, by substitution and simplification into Eq. (16):

$$\begin{aligned} W' &= \frac{1}{2} [(L_{sa} - L_{uu}) i_r^2 + (L_{ua} - L_{sa}) i_s i_r + c \cdot \Psi_s i_r - c \cdot \Psi_s i_s] = \\ &= \frac{1}{2} \left[ 2 \cdot V_{rms(PWM)} \frac{c \cdot \beta s}{\omega} \cdot i_r + (L_{uu} - L_{sa}) i_r^2 - \frac{(V_{rms(PWM)} \frac{c \cdot \beta s}{\omega} + (L_{uu} - L_{sa}) \cdot i_r)^2}{L_{ua} - L_{sa}} \right] \end{aligned} \quad (23)$$

Eq. (23) is the fundamental expression for the computation of the energy conversion  $W'$  for any SR machine, including both saturating and non-saturating cases, as well as for the trapezoidal phase current profile operation [6] and for the general quadrilateral operation of the phase currents as in **Figure 11** and for the motoring and the generating modes of the machine operation. By comparison, Eq. (23) indicates significantly different behavior of the general SR machine case compared to the special cases in Eqs. (5) and (7).

The questions remain as to how to estimate the commutation factor  $c$  and the *rms* voltage, since Eq. (23) requires these numeric values to be assumed in order to calculate accurately the energy conversion area  $W'$ , whereas only the DC bus voltage and the rated current are given (or are assumed to be known in the design process) as in **Table 1**. Considering **Figure 12**, corresponding to **Figure 11**, where the  $c$  factor is shown graphically, we assume that—strictly for the rated motor speed—the commutation of the phase current profile starts at point C, which is well before the rotor pole is fully aligned with the stator pole, and this is so that the current can be brought down in the shortest time possible to point E so as to maximize the torque-generating region.

Assuming that, first of all, the phase current reaches point A with the full wave DC bus voltage when the rotor is at the unaligned position, but also with the early commutation assumption in mind, we determine the time taken for the rated current  $i_r$  to fall to the saturation value  $i_s$ , from Eq. (11) and **Figure 11**, which is approximately

$$\begin{aligned} \Psi_{sa}(@B) - \Psi_{sa}(@D) &= (0.0004948(H) \times 320 (Amp) + 0.4192920(V \cdot s)) \\ &\quad - (0.0004948(H) \times 62.6 (Amp) + 0.4192920(V \cdot s)) \\ &= 0.12736 (V \cdot s) \end{aligned} \quad (24)$$

Moreover, since the steady angular speed and the DC bus voltage at the point of the commutation are known, the time required for the current to fall from point C to point E in **Figure 12** is

$$\frac{\Psi_{sa}(@B) - \Psi_{sa}(@D)}{V_{DC}} = \frac{0.12736 (V \cdot s)}{500 (V)} = 2.547 \times 10^{-4} (s) \quad (25)$$



since the full wave voltage is applied as in **Figure 3**.

Therefore, the angle through which the rotor traverses during this time period can be found, since the rated angular speed is known:

$$\begin{aligned}\theta_{CE} &= \frac{\Psi_{sa}(@B) - \Psi_{sa}(@D)}{V_{DC}} \times \omega = \frac{0.12736 \text{ (V} \cdot \text{s)}}{500 \text{ (V)}} \times \frac{1200 \text{ (rpm)}}{60} \times 2\pi \\ &= 0.032 \text{ (radians)} = 1.83 \text{ (degrees)}\end{aligned}\quad (26)$$

Finally, from the definition of the commutation factor  $c$  in **Figure 12**, we find:

$$c = 1 - \frac{\theta_{CE}}{\beta_s} = 1 - \frac{1.83 \text{ (degrees)}}{10.5 \text{ (degrees)}} \approx 0.8 \quad (27)$$

Also of interest is the *rms* voltage that is applied across the phase winding when the peak current is flat-topped as in **Figure 12**; this current shape is assumed to be present at the rated motor speed. Therefore the *rms* voltage from point A to point C in **Figure 12**, using Eq. (19), is

$$V_{rms(PWM)} = \left( \Psi_s + (L_{sa} - L_{uu}) \cdot \frac{i_r}{c} \right) \frac{\omega}{\beta_s} \approx 100 \text{ (V)} \quad (28)$$

being only an approximate value since the winding resistance voltage is assumed to be unknown at this stage of analysis which would be added to the *rms* voltage.

Having estimated the commutation factor and the *rms* voltage, Eq. (23) is used to find the energy conversion capability of the chosen SRM2 machine at the rated angular speed of 1200 rpm and the other variables taken from **Table 1** and **Figure 9**, for a single phase:

$$\begin{aligned}W' &= \frac{1}{2} \left[ 2 \cdot V_{rms(PWM)} \frac{c \cdot \beta_s}{\omega} \cdot i_r + (L_{uu} - L_{sa}) i_r^2 - \frac{(V_{rms(PWM)} \frac{c \cdot \beta_s}{\omega} + (L_{uu} - L_{sa}) \cdot i_r)^2}{L_{ua} - L_{sa}} \right] \\ &= \frac{1}{2} [74.67 + 72.95 - 17.74] \approx 65 \text{ (Joules)}\end{aligned}\quad (29)$$

The total torque at the rated speed of the three-phase,  $q$ , SRM2 machine is thus estimated as follows:

$$T = W' \times \frac{q \cdot N_r}{2\pi} = 65 \times \frac{3 \times 12}{2\pi} \approx 372 \text{ (N} \cdot \text{m)} \quad (30)$$

The analytically calculated rated torque value of the chosen SRM2 SR machine compares favorably with the published measured rated torque value of 400 Nm, being about 8% underestimated. This small discrepancy arises since our calculations in Eq. (29) are influenced by two main factors as a consequence of the simplifications made. First—and this has an overestimating effect—the excursion of the phase current into the decreasing inductance region after the full stator and rotor alignment,  $EF$  in **Figure 12**, is considered in Eq. (23) as a positive torque generation region, whereas in reality it is a negative torque generation region. Secondly—and this leads to the underestimating effect in Eq. (29)—generally there is the phase overlap present, as in **Figure 3**, where a fraction of a leading phase energy conversion is being compensated by a fraction of the trailing phase which, if accounted for, increases the instantaneous torque in Eq. (23). Therefore, by accounting for the SRM2 machine phase overlap ratio  $R$  at the rated speed, we are able to compensate

for the underestimated torque generation value in Eq. (29) for the overlapping torques:

$$R = 1 + \frac{1}{\beta_s} \left( \beta_s - \left( \frac{360}{N_r} - \frac{360}{N_s} \right) \right) = 1.0476 \quad (31)$$

where the stator pole arc angle  $\beta_s$  is in mechanical degrees and  $N_s$  and  $N_r$  are the number of the stator and the rotor poles, respectively. The answer of Eq. (31) can now be multiplied by the computed torque value of Eq. (30) which makes the discrepancy with respect to the published measured torque of less than about 3% underestimated, which must be considered as relatively very accurate for the analytical method-based design process.

Other factors influencing the accuracy of the analytical torque calculations include the uncertainties in the estimated commutation factor  $c$  as well as the actual *rms* voltage, both not reported in [4]. However, the published maximum computed torque value in [4] was in the region of 415 (N·m) at the assumed 1200 (rpm) rated speed, as in **Table 1**. The reasons for the discrepancy between the reported measured and the reported computed rated torque values in [4] were not explained.

Finally, the electromechanical power at the rated speed for the SRM2 design can be estimated as

$$P_{em} = T \times \omega = W' \times \frac{q \cdot N_r}{2\pi} \times \omega \times R \approx 390 \text{ (N} \cdot \text{m)} \times \frac{1200 \text{ (rpm)}}{60} \times 2\pi = 49 \text{ (kW)} \quad (32)$$

which is an underestimate of about 2% compared to the published power levels at the rated speed [4]. However, the maximum power of the SRM2 design beyond the rated speed was quoted as 54 (kW).

Although Eq. (23) (or Eq. (29)) is rather complex, it represents the most suitable form of Eq. (16), since the numerical evaluation of all flux-linkage values, term by term, at each desired phase current level is no longer required. Even more importantly, Eq. (23) is very convenient to use as the operating parameters that are readily available to machine designers are typically expressed in terms of the inductance estimates, obtained either from finite element analysis or the analytic aligned and unaligned flux-linkage maps. Furthermore, the theory of other electric machines usually relies on inductances, and for this reason, Eq. (23) can be more accessible and intuitive for the control engineers.

The required operating parameters to be used in Eq. (23) for the fundamental energy conversion estimation of the SR machine are collected from **Figure 9** and Eqs. (27) and (28) and are summarized in **Table 2**.

Eq. (29) is further exploited to gain insights into the torque control effectiveness of the saturable SR machines via the rated phase current regulation. The operating parameters from **Table 2** were substituted into Eqs. (29) and (30), and the rated phase current was varied from some minimum practical value to the full rated phase current value, as plotted in **Figure 13**.

**Figure 13** reveals critically important results regarding saturable SR machine operation when, at the fixed constant speed, the torque is regulated with the phase current only. If the start of the phase current rise is to be fixed at a certain rotor angle,  $\theta_{on}$  in **Figure 12**, and the current decay should start at the commutation angle,  $\theta_{com}$ , the electromagnetic torque production for the SR machine will be weakly nonlinear and will follow the power law in phase current as in **Figure 13**. This is significant from the control point of view since—if the linear torque control is to result from the linear increase of the phase current—the current will have to be

Energy conversion variables to be used in Eq. (23)	
Required SR machine design parameters:	50 kW SRM2
Saturated aligned inductance, $L_{sa}$ [H]	0.0004948
Unsaturated aligned inductance, $L_{ua}$ [H]	0.0071879
Unsaturated unaligned inductance, $L_{uu}$ [H]	0.0012072
Stator pole arc angle $\beta_s$ [degrees]	10.5
Rated angular speed $\omega$ [rad/s]	125.7
Rated current, $i_r$ [A]	320
rms voltage, $V_{rms(PWM)}$ [V]	100
DC bus voltage [V]	500
Commutation factor $c$	0.8

**Table 2.**  
50 kW SRM2 machine parameters.

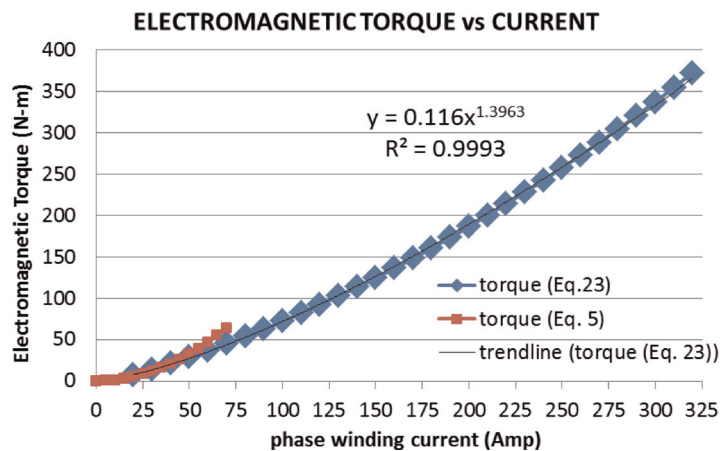


**Figure 13.**  
The electromagnetic torque production as a function of the phase current regulation.

regulated simultaneously with the turn-on and the commutation angles, as defined in **Figure 12**. Therefore, for each required torque value at the fixed constant speed, an exhaustive search for the combination of the three control parameters will have to be performed, that is, the turn-on, the commutation, and the phase current magnitude. This type of search is effective only with the help of computer-based design routines; for example, see [8, 10].

**Figure 13** also shows the torque obtained from Eq. (5) where the linear non-saturating SR machine is assumed for all rated current values. The linear theory suggests that the torque production follows the quadratic power law with the phase current, as is also evident from Eq. (5) itself. The torque values in the region below the saturation current are similar using both methods; however, once the current is increased beyond the saturation level, the linear theory overestimates the torque value and becomes invalid. To conclude, the general torque of the saturable SR machine can be computed relatively quickly and accurately with Eq. (23), even if the rated phase current value is reduced below the saturation current value.

Further discussion regarding Eq. (23) is as follows. It should be understood that the commutation factor  $c$ , as computable with Eq. (27), is not a constant but can be chosen or optimized, depending on the commutation timing as in **Figure 12**.

Likewise, the *rms* voltage is not a constant, as computable with Eq. (28), but is dependent on the commutation factor and the rated speed. The terms of Eq. (23) can be examined in turn in order to gain further insights into the operation and energy conversion process of the general SR machine.

The first term in Eq. (23), the “voltage” term,

$$2 \cdot V_{rms(PWM)} \frac{c \cdot \beta s}{\omega} \cdot i_r \quad (33)$$

indicates that the energy conversion part of this term is dominated by the rated current and the commutation factor; however, even with zero commutation factor, the machine will produce some useful torque, since the full wave DC bus voltage is still utilized, while with the *c* factor equal unity, the *rms* voltage-based energy component will be fully realized. Moreover, the *rms* voltage will tend to increase the energy conversion component, itself being a function of the operating speed at which it occurs. The *rms* voltage is created by the power electronic switches as shown in **Figure 3**.

The second term in Eq. (23), the “inductance” term,

$$(L_{uu} - L_{sa}) i_r^2, \quad (34)$$

contributes significantly to the energy conversion process and is dominated by the square of the rated current in the phase winding. Therefore, it is desirable to maximize this value in order to operate at the highest possible torque, yet giving proper consideration to the cooling requirements of the SR machine, as at very high phase current values, the cooling of the windings becomes very challenging. It therefore appears that in order to arrive at a torque dense SR machine design, as the main goal, it is important to drive as large a current through the motor windings as is practicable. Furthermore, the inductance difference  $L_{uu} - L_{sa}$  should be made as large as possible. This can be achieved in practice if the saturated aligned inductance  $L_{sa}$  is minimized with respect to the unsaturated unaligned inductance  $L_{uu}$ .

The third term in Eq. (23), the “saturation quality” penalty term,

$$\frac{(V_{rms(PWM)} \frac{c \cdot \beta s}{\omega} + (L_{uu} - L_{sa}) \cdot i_r)^2}{L_{ua} - L_{sa}}, \quad (35)$$

is a relatively large negative quantity and is dominated by the denominator defined by the inductance difference. Therefore, to reduce this “penalty,” it would be desirable to maximize the unsaturated aligned inductance  $L_{ua}$ , while the saturated aligned inductance  $L_{sa}$  should be kept as low as possible in relation to the unsaturated aligned inductance. This effect can only be achieved with the highest-quality electric steels, having very high saturation flux density values, which must therefore be used to make the core of the SR stator and rotor [7].

## 2.2 Saturable switched reluctance machine energy conversion ratio estimation

Since the SR machine requires a DC bus capacitor if the DC supply voltage is to be kept undisturbed by the returning magnetic field energy from the phase windings, as discussed and shown in **Figure 2**, the estimation of the magnitude of such returning energy is an important consideration when designing the h-bridge power electronic converter for the SR machine. As was shown in **Figure 10**, which for convenience is replotted here as **Figure 14**, the magnetic field energy  $W_f$  first increases as the phase current rises in the phase windings up to point *B*, at which point it is returned as the phase current is commutated to decay to zero.

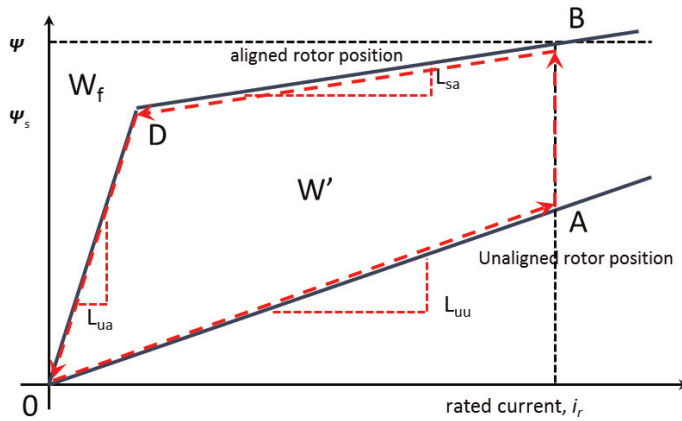


**Figure 14.** Linearized flux-linkage curves for the 18/12 SRM2 and the definition of the magnetic field energy  $W_f$ .

The amount of energy (in joules) being created as a result of the phase current (and the magnetic field in the windings) build-up is represented by the area bounded by the entire aligned flux-linkage curve, the horizontal line at point *B* at which the maximum flux-linkage is being established by the current profile as shown in **Figure 14** and by the flux-linkage axis thus being a quadrilateral.

Knowing the magnitude of the stored magnetic field energy  $W_f$  in the phase winding at the rated speed of the SR machine enables the energy conversion ratio [6] to be determined as

$$\text{energy conversion ratio} = \frac{W'}{W' + W_f} \quad (36)$$

In order to estimate the energy conversion ratio, it is necessary to estimate the stored magnetic field energy  $W_f$  along the lines of Eq. (23) and **Figures 9** and **10** with the help of Varignon parallelogram calculations. Detailed derivation is not shown here to save space, but readers are encouraged to verify the following result:

$$W_f = \frac{1}{2} \left[ L_{sa} \dot{i}_r^2 + \frac{(V_{rms(PWM)} \frac{c\beta s}{\omega} + (L_{uu} - L_{sa}) \cdot \dot{i}_r)^2}{L_{ua} - L_{sa}} \right] \quad (37)$$

Eq. (37), being somewhat less complex than Eq. (23), can be interpreted as follows: maximizing the rated current and the saturated aligned inductance,  $L_{sa}$ , will greatly increase the stored magnetic field energy. Furthermore, minimizing the difference between the inductances in the identified “saturation penalty” term in Eq. (37) will help to minimize the stored magnetic field energy, which is a desirable effect and can be achieved by selecting the electric steel with high saturation flux density values for the construction of the SR machine.

Substituting the known operating parameters of the SRM2 design from **Table 2**, the estimated field energy is found as

$$W_f = \frac{1}{2} \left[ 50.67 + \frac{0.1354}{0.0067} \right] \approx 35.5 \text{ (joules)} \quad (38)$$

Using Eq. (37) for the operating parameters from **Table 2**, with the phase current magnitude varied from some lower practical limit to the full rated current, the energy conversion ratios were obtained with Eq. (36) as shown in **Figure 15**.

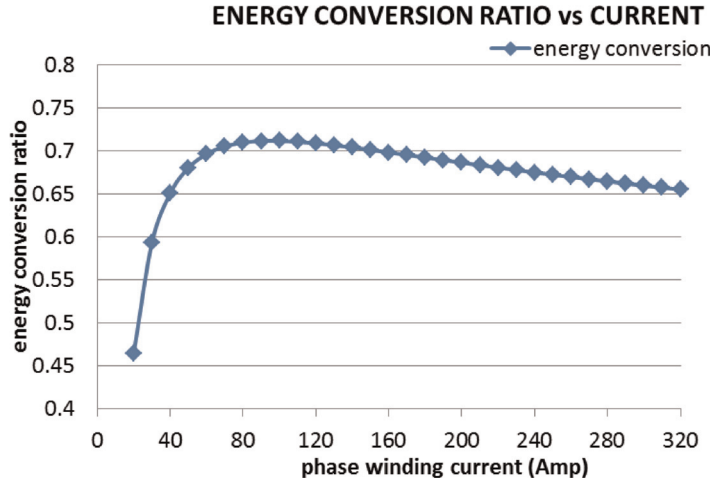


Figure 15.

Energy conversion ratio curve for the 18/12 SRM2, for the rated speed of 1200 (rpm).

From **Figure 15** it is seen that the amount of the energy converted by the SRM2 design is rather small at the low phase current values, but it improves quickly as the phase current increases, in effect encompassing more of the co-energy area  $W'$  as in **Figure 14**. However, there is a definite optimum phase current value above which the energy conversion ratio starts to decrease again, and this phase current value is well below the rated current. The reason as to why the energy conversion ratio is decreasing as the phase current is increased is due to the uneven incremental co-energy areas  $\Delta W'$  being encompassed by the phase current profile with respect to the incrementally increased stored magnetic field energy  $\Delta W_f$  being created, thus having the diminishing effectiveness as in **Figure 15** and given by Eq. (36), although this effect is not too severe for the most useful range of the currents.

### 2.3 Saturable switched reluctance machine average rated current and voltage estimation

Having successfully obtained the rated torque values for the selected SRM2 machine design using Eq. (29), we are now in a position to extend the analytical treatment for the estimation of the average rated phase current as well as the voltage. These quantities are very important during the preliminary SR machine design process in order to estimate the demand from the available DC bus supply, such as a battery of an electric vehicle. Furthermore, the knowledge of the rated current is required for the estimation of the heat dissipation requirements for the designed SR machine.

Consider **Figure 12**, which for convenience is redrawn here as **Figure 16**.

Since by using Eqs. (24) to (28) we were able to evaluate the commutation factor  $c$  and the *rms* voltage, similar reasoning will be applied to find the rest of the information needed to estimate the rated average phase current. The aim is to use the Varignon parallelogram principles as in **Figure 10** to compute the area of the quadrilateral  $OFEC$  in **Figure 16** as well as the triangular areas  $\theta OA$  and  $OCA$ .

To find the time it takes for the phase current to rise to the rated value, using Eq. (25),

$$t_{\theta \rightarrow O} = \frac{\Psi_{uu}(@A) - 0}{V_{DC}} = \frac{0.3863 (V \cdot s)}{500 (V)} = 7.73 \times 10^{-4} (s) \quad (39)$$



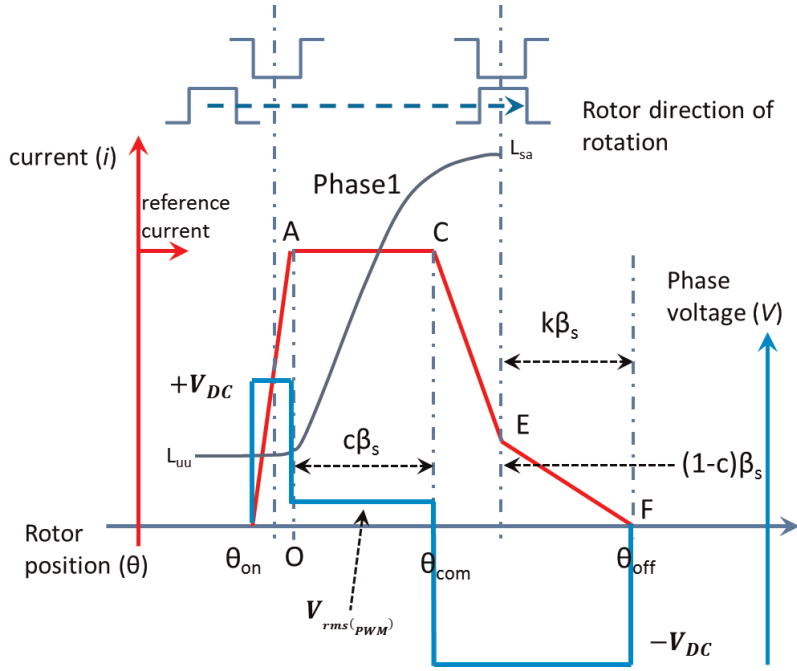


**Figure 16.**  
 Phase current profile in the phase windings as a function of the voltages and rotor position angles.

For the rotor to traverse from point A to point C, as in **Figure 16**,

$$t_{A \rightarrow C} = \frac{\Psi_{sa}(@D) - \Psi_{uu}(@A)}{V_{rms(PWM)}} = \frac{0.1074 (V \cdot s)}{100 (V)} = 1.074 \times 10^{-3} (s) \quad (40)$$

where the saturated aligned flux-linkage at D is

$$\Psi_{sa} = L_{sa} \cdot i_r + c \cdot \Psi_s = 0.0004948i_r + 0.8 \times 0.4192920 \quad (41)$$

Next we estimate the time needed for the phase current to decay from point E to point F, the  $k \cdot \beta_s$  factor, at which it is zero as in **Figure 16**:

$$t_{E \rightarrow F} = \frac{\Psi_{ua}(@E)}{V_{DC}} = \frac{0.3701 (V \cdot s)}{500 (V)} = 7.40 \times 10^{-4} (s) \quad (42)$$

where the saturating current needed to evaluate the unsaturated aligned flux-linkage in Eq. (42) was found from Eq. (22) using  $c = 0.8$  as before:

$$i_s = \frac{V_{rms(PWM)} \frac{c \cdot \beta_s}{\omega} - (L_{sa} - L_{uu})i_r}{L_{ua} - L_{sa}} \approx 51.5 (A) \quad (43)$$

Finally, the time from C to E was estimated earlier using Eq. (25) as

$$t_{C \rightarrow E} = 2.547 \times 10^{-4} (s) \quad (44)$$

Thus the area bound by the quadrilateral OFEC can be found, as in Eq. (14):

$$\begin{aligned} A_{OFEC} &= \frac{1}{2} [(t_{A \rightarrow C} + t_{C \rightarrow E}) \times i_r + (t_{C \rightarrow E} + t_{E \rightarrow F}) \times i_s] = \\ &= 0.2381 (A \cdot s) \end{aligned} \quad (45)$$

The triangular area  $OAC$  and  $\theta OA$  are easily found as

$$A_{OAC} = \frac{1}{2} [t_{A \rightarrow C} \times i_r] = 0.17184 \text{ (A} \cdot \text{s)} \quad (46)$$

and

$$A_{\theta OA} = \frac{1}{2} [t_{\theta \rightarrow O} \times i_r] = 0.12368 \text{ (A} \cdot \text{s)} \quad (47)$$

Now the areas are added and divided by the total rotor traverse time from  $\theta_{on}$  to  $\theta_{off}$  in **Figure 16**, to obtain the average phase current:

$$I_{AV} = \frac{0.53362 \text{ (A} \cdot \text{s)}}{0.0028417 \text{ (s)}} \approx 188 \text{ (A)} \quad (48)$$

However, by revisiting the argument regarding the overlapping phase operation of the selected SRM2 machine at the rated speed, we make use of the overlap ratio  $R$  defined in Eq. (31) in order to obtain a more conservative estimate of the average rated *rms* phase current expected to be demanded from the battery (see **Table 1**):

$$I_{BAT} = I_{AV} \times R = \frac{0.53362 \text{ (A} \cdot \text{s)}}{0.0028417 \text{ (s)}} \times 1.045 \approx 196 \text{ (A)} \quad (49)$$

Likewise, all of the information needed to compute the average phase voltage from the known instantaneous voltage waveform of **Figure 16** is readily available. The computed value found for the single phase at the rated speed is

$$V_{AV} \approx 350 \text{ (V)} \quad (50)$$

Therefore, at the rated speed, the SRM2 machine will be demanding the electric power:

$$P_{EL} = I_{BAT} \times V_{AV} = 196 \text{ (A)} \times 350 \text{ (V)} = 68 \text{ (kW)} \quad (51)$$

The result in Eq. (51) does not need to include the power factor at the rated speed since the phase currents and voltages are averaged over the full electrical cycle in Eqs. (49) and (50). Finally, knowing the demanded electric power and the generated electromagnetic power, the efficiency of the SR machine at the rated speed can be readily found which for this particular case is:

$$Efficiency = \frac{49 \text{ (kW)}}{68 \text{ (kW)}} \approx 72\% \quad (52)$$

which compares favorably with the published efficiency value of around 80% at the rated speed and torque [4].

The above estimated electric power demand compares well with the electromagnetic power production as found in Eq. (32). Therefore, the relatively accurate SR machine design process is accomplished.

## 2.4 Saturable switched reluctance machine converter volt-ampere requirement estimation

As was shown in **Figure 2**, the asymmetric h-bridge SR machine power electronic converter requires two active devices (transistor switches) and two passive

devices (the power diodes per single phase) in order to realize the most flexible SR machine operation in a motoring mode or a generating mode [7]. Consequently, we can define the metric of the volt-ampere product that these power electronic devices have to be rated at in order to deliver the required phase current at the required DC bus voltage.

For a three-phase,  $q = 3$ , SR machine operated from a fixed supply DC bus voltage,  $V$ , and off the asymmetric half-bridge power electronic converter delivering the phase current,  $i$ , the maximum volt-ampere rating of the power electronic converter is defined as [6]

$$S = 2q \cdot Vi = 2 \times 3 \times 500(\text{V}) \times 350(\text{A}) = 1050(\text{kVA}) \quad (53)$$

Eq. (53) indicates that the stated maximum of the current will have to be delivered by the transistor switches having the stated voltage rating. The quantity obtainable with Eq. (53) is in units of kVA, and in this case, it is permissible to form a ratio of two quantities not having the same units [6] as long as both units are explicitly retained, and thus the converter volt-ampere value in Eq. (53) is divided by the produced electromagnetic power, as computed with Eq. (32), to obtain a measure of economic utilization of the converter in terms of kVA/kW:

$$S/P = \frac{4\pi \cdot Vi}{W'N_r} \quad (\text{kVA/kW}) \quad (54)$$

where the volt-ampere quantity  $S$  is a constant and the electromagnetic power is computed from Eq. (32) with the current taken as a parameter. The ratio is then computed with Eq. (54) for the range of phase current values  $i$  and is plotted in **Figure 17** for the fixed constant rated speed of 1200 (rpm) for the SRM2 machine.

**Figure 17** shows the h-bridge converter volt-ampere requirement for the rated angular speed of 1200 (rpm) with the phase current as a parameter. The curve in **Figure 17** indicates that approximately 25 (kVA/kW) rating is required at the power electronic converter end of the SR machine drive in order to deliver the rated torque, as found in the previous section using Eqs. (29) and (30). As the phase current magnitude is reduced in order to reduce the torque level, while the angular speed is kept constant, the  $S/P$  ratio tends to increase slowly first, but as the current

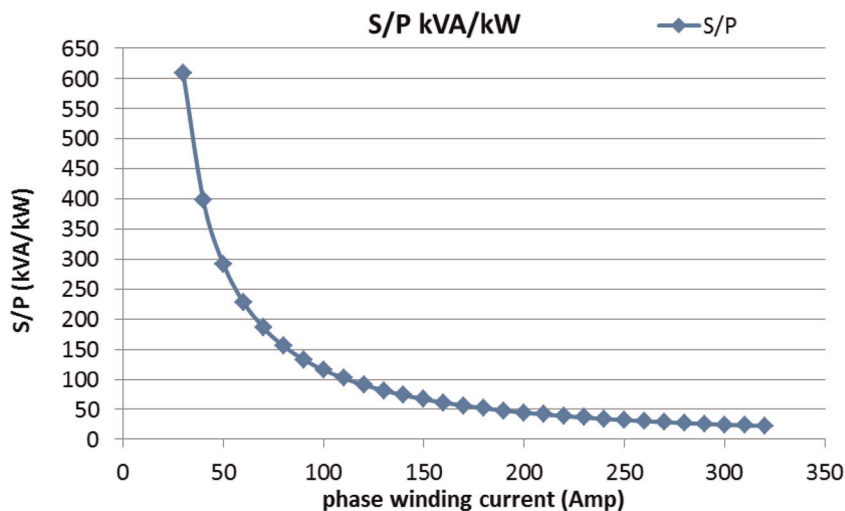


**Figure 17.**  
Converter volt-ampere requirement curve for the 18/12 SRM2, for the rated speed of 1200 (rpm).

is reduced to a very low value, the ratio becomes very large. This trend only suggests the operating penalty when the demanded torque is low; however, the maximum rated torque operation of the saturable SR machine makes very clear economic sense compared to the non-saturating SR machine in terms of the size of the power electronic converter for the given amount of rated torque production [6]. Therefore, the saturable SR machine can be constructed economically since the power electronic transistors and diodes increase in price as their volt-ampere rating (kVA) is increased.

## 2.5 Saturable switched reluctance machine generator mode energy conversion estimation

Since SR machines are able to operate in the motoring as well as the generating mode, the energy conversion performance of an SR generator will also be quite accurately predicted with the Varignon parallelogram theorem as was the case for the motoring mode given by Eq. (23).

Consider **Figure 10** where for the SR machine-generating mode the locus of the phase current is reversed. Therefore the phase current will form the quadrilateral  $V_0V_3V_2V_1V_0$  since the phase current will start flowing just before the rotor pole is aligned with the stator pole. The co-energy area  $W'$  for the generator encompassed by the phase current locus will be given in terms of the vector coordinates along the lines of Eq. (15), but with the vector sequence reversed, thus:

$$W' = \frac{1}{2}[(i_r - 0)(\Psi_{uu} - \Psi_{ua}) - (i_r - i_s)(\Psi_{sa} - 0)] \text{ (Joules)} \quad (55)$$

Having the co-energy relation for the generator, we then make use of Eq. (19) and Eq. (22) to express the generator co-energy in Eq. (55) in terms of the inductances, rated phase current, and *rms* voltage:

$$\begin{aligned} W' &= \frac{1}{2}[(L_{uu} - L_{sa})i_r^2 + (L_{sa} - L_{ua})i_s i_r + c \cdot \Psi_s i_s - c \cdot \Psi_s i_r] = \\ &= \frac{1}{2} \left[ -2 \cdot V_{rms(PWM)} \frac{c \cdot \beta s}{\omega} \cdot i_r - (L_{uu} - L_{sa})i_r^2 + \frac{(V_{rms(PWM)} \frac{c \cdot \beta s}{\omega} + (L_{uu} - L_{sa}) \cdot i_r)^2}{L_{ua} - L_{sa}} \right] \end{aligned} \quad (56)$$

Eq. (56) is the fundamental expression for the computation of the energy conversion  $W'$  for any SR generator, both saturating and non-saturating cases, as well as for the trapezoidal phase current profile operation [6] and for the general quadrilateral operation of the phase currents as in **Figure 11**.

The *rms* voltage and the commutation factor for the generating mode are both found from Eq. (27) and Eq. (28), and the generated average phase current will be found as in Section 2.3. Such generated DC current will be possible only if the external torque is applied to the SR generator, and the magnitude of such torque requirement as given in Eq. (56) and Eq. (30) will be a negative quantity, indicating that the external torque input is required.

## 3. Conclusions

Having successfully found the rated torque and power production capability of the analyzed SR machine design, we are now in the position to summarize the

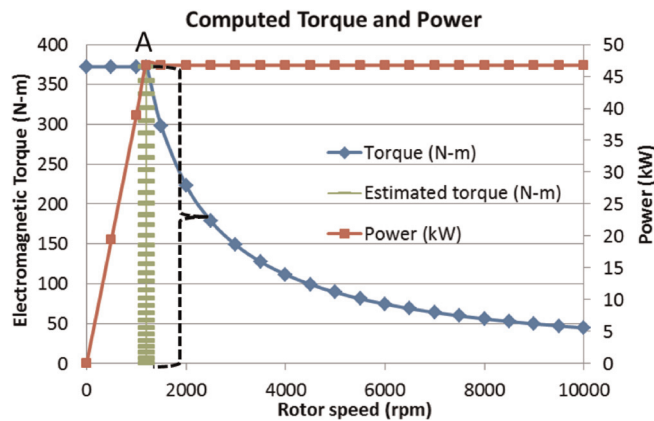


**Figure 18.**  
 Estimated speed-torque and speed-power characteristics for the analyzed SR machine design.

advantages of the proposed analytic method based on Varignon parallelogram and vector-based computations.

The estimated rated torque and power of a general SR machine are the two most important quantities a machine designer is seeking at early stages of the machine design process. Once these two estimates are known for the required rated speed, the speed-torque and power-torque characteristics for the SR machine can be constructed as in **Figure 18**.

The particular characteristics in **Figure 18** are assumed to obey the constant-torque and constant-power operation of the SR machine with respect to the speed of rotation. Such specific characteristics are most desirable from the accurate torque and power control point of view and are used for electric vehicle propulsion applications or the general industrial motor drive applications.

The convenient analytical form of Eq. (23) enables the SR machine design engineer to estimate relatively accurately the electromagnetic torque of the machine at the assumed required rated speed, at point A in **Figure 18**, which in turn is dictated by the particular practical application. Furthermore, this electromagnetic torque is estimated with the known (or application dictated) quantities such as DC bus voltage, rated current, and the geometric parameters of the assumed SR machine design. More importantly, the SR machine design engineer is able to parametrize Eq. (23) in terms of the phase current in order to estimate the range of the rated torque with respect to the change in the phase current magnitude as indicated by the bracket in **Figure 18**. At this stage of the SR machine design process, the engineer has enough information to construct the constant-torque and constant-power characteristic curves, as in **Figure 18**, with the help of Eq. (32). Such a characteristic map can be enhanced with further operating quantities of the average phase winding current and average voltage. The other performance metrics for the designed SR machine to be estimated with the help of the proposed analytical method are the volt-ampere requirements of the power electronic converter for the SR machine being designed. This entire information regarding the designed SR machine enables the decision-making process if such SR machine is to be further analyzed in more detail, this time with advanced computer-based optimization routines [8].

## **Author details**

Aleksas Stuikeys<sup>1\*</sup> and Jan Sykulski<sup>2</sup>


1 RETORQ Motors Ltd., London, UK

2 Electronics and Computer Science, University of Southampton, Southampton, UK

\*Address all correspondence to: a.stuikys.ac@gmail.com

## **IntechOpen**

---

© 2019 The Author(s). Licensee IntechOpen. Distributed under the terms of the Creative Commons Attribution - NonCommercial 4.0 License (<https://creativecommons.org/licenses/by-nc/4.0/>), which permits use, distribution and reproduction for non-commercial purposes, provided the original is properly cited. 



## References

- [1] Nasar SA. D.C.-switched reluctance motor. Proceedings of the Institution of Electrical Engineers. 1969;**116**(6):1048
- [2] Widmer JD, Martin R, Kimiabeigi M. Electric vehicle traction motors without rare earth magnets. Sustainable Materials and Technologies. 2015;**3**:7-13
- [3] Krishnan R. Switched Reluctance Motor Drives: Modeling, Simulation, Analysis, Design, and Applications. Boca Raton, FL: CRC Press; 2001
- [4] Takeno M, Chiba A, Hoshi N, Ogasawara S, Takemoto M, Rahman MA. Test results and torque improvement of the 50-kW switched reluctance motor designed for hybrid electric vehicles. IEEE Transactions on Industry Applications. 2012;**48**(4): 1327-1334
- [5] Meeker D. Finite Element Method Magnetics (FEMM), FEMM Reference Manual. Available from: <http://www.femm.info/wiki/Documentation/> [Accessed: 5 September 2017]
- [6] Miller TJE. Converter volt-ampere requirements of the switched reluctance motor drive. IEEE Transactions on Industry Applications. 1985;**IA-21**(5): 1136-1144
- [7] Miller TJE. Switched Reluctance Motors and Their Control. Hillsboro, OH/Oxford: Magna Physics Pub.; Clarendon Press; 1993
- [8] Stukys A, Sykulski J. Rapid multi-objective design optimization of switched reluctance motors exploiting magnetic flux tubes. IET Science Measurement & Technology. 2017
- [9] Coxeter HSM, Greitzer SL. Geometry Revisited, 10. print. Mathematical Association of America: Washington; 2005
- [10] Stukys A, Sykulski JK. An efficient design optimization framework for nonlinear switched reluctance machines. IEEE Transactions on Industry Applications. May 2017;**53**(3): 1985-1993